Rutherford Scattering

Parker Lewis
Amadie Wijenarayana
Ohio University
Department of Physics and Astronomy, Athens, OH, 45701, USA

December 14, 2024

Abstract

This lab report presents the findings of Rutherford's scattering experiment conducted at the Edwards Accelerator on the Ohio University campus. The experiment involved directing a ${}^{4}_{2}He^{2+}$ beam at a metal foil to study the scattering effects. The lab had three primary objectives: to perform energy calibration, confirm the composition of the foil, and compare theoretical and experimental differential cross-sections at various angles. The results indicated that the energy calibration produced residuals between -0.1 to 0.1 MeV, with a residual plot resembling a constant line. The foil composition was determined to be gold at $79.3 \pm 1.1\%$, silver at $10.99 \pm 0.63\%$, and copper at $9.7 \pm 0.94\%$. These values suggest that the measured composition fell within 0.1σ to 1σ of the desired proportions of 80%, 10%, and 10% for gold, silver, and copper, respectively. Regarding the theoretical and experimental cross-sections, only gold peaks were evaluated. Both exhibited a dependence on $\sin^{-4}(\theta/2)$, thereby confirming the validity of the Rutherford model after correcting systematics dead times. Furthermore, a ratio plot comparing the experimental and theoretical cross-sections was created for absolute angles. This plot indicated that the approximate ratio of all values converged around $R_{exp/theo} = 0.7$, revealing a discrepancy of only 30% between the experimental and theoretical cross-sections [1]. [Counts: 207]

1 Theory/Intro

1.1 Lab Overview/Topics

In this chapter of the lab report, an overview of the lab objectives and tasks will be presented, along with a discussion of the theory underlying the experiment. The class was divided into groups to perform offline analysis for Rutherford scattering data, focusing on varying energy or angles. The general overview is as follows: pre-run measurements of known quantities required for offline analysis were performed on the first day. On the second day, Rutherford scattering data was collected at varying angles. On the final day, data collection focused on varying energy[1]. The

concluding step involved offline analysis, including energy calibration, composition confirmation, and comparison between theoretical and experimental results. The experimental and analysis chapters will provide more detailed explanations of these steps. The remainder of this section will establish the theoretical foundations of Rutherford Scattering. Topics covered include explaining what a scattering experiment entails and introducing the statistical definitions of cross-sections and differential cross-sections. [Counts: 164]

1.2 Scattering/Cross-Section Theory

Before we define a differential cross-section, let's start defining a scattering experiment. A scattering experiment comprises two objects of interest in the whole system of said experiment: the incoming projectile beam and the target apparatus. The projectile beam can be anything you shoot toward the target, but in all but most cases for scattering experiments, it will always be composed of subatomic particles like alphas, electrons, any ion type, hadrons, etc. The target can be stationary or moving. This is based on the frame of the experiment and how it's designed, but I will get into that discussion in a bit. The target is also made up of groups of subatomic particles like the list discussed above. Still, stationary scattering experiments usually involve the nuclei of specific atom species, such as a gold nucleus. In this lab, the target combined the composition of gold, silver, and copper nuclei that made up the foil, and the projectile was a beam of alphas. As a projectile with its line of approach will either hard scatter with a much heavier target, which will then change the path of the incident beam at a certain point, the target-induced field (ex. Electromagnetic Repulsion) will eject the incident beam of particles and change its path this is what all scattering experiments are [2]. Scattering experiments are done so that the internal structure of atoms, interactions between projectile/target, and matter confirmation are proven/shown. A cross-section is essentially defined as the effective area of a target; here's the catch in most experiments, especially in subatomic collisions: the shape of the target is unknown [3]. A new definition of a cross-section has to be used, and it's actually defined as the statistical likelihood that a specific interaction occurs in an experiment with the incident beam and target. The interaction potential and statistics of the target/incident beam are what give the shape of the target. In the Rutherford Model, the potential that describes the process is the Coulomb Potential [3]. A differential cross-section is a probability that a specific interaction subtends the specific solid angle orientation of the target[3]. In this lab, the governing equation is defined as:

$$N_{\text{sc}} = N_{\text{inc}} n_{\text{tar}} \frac{d\sigma}{d\Omega}(\theta, \phi) d\Omega. \tag{1}$$

Specifically, Eq. 1 defines how to determine the differential cross-section experimentally given the incident particle beam count, number of scattering centers, target density, and solid angle. The Rutherford Cross-section in this lab is defined as:

$$\frac{d\sigma}{d\Omega} = 1.296 \left(\frac{Z_0 Z_1}{E_0}\right)^2 \left[\frac{1}{\sin^4\left(\frac{\theta}{2}\right)} - 2\left(\frac{M_0}{M_1}\right)^2\right] [\text{mb MeV}^2\ \text{sr}^{-1}]. \tag{2}$$

This version of the Rutherford Model is defined in nuclear physics units. Mass terms of index 0 and 1 represent the target and projectile masses, atomic number Z from both terms defines the

projectile and target charge, and E is the incident beam energy. Final thoughts from Eq. 2 are that the cross-sections are measured in the lab frame. [Counts: 483]

2 Equipment/Procedure

In this section, all the components used to run the experiment for each day run will be discussed, along with pre-run measurements, a description of trial run days, and how the raw data was displayed. [Counts: 34]

2.1 Equipment Pieces

A quick overview of the experiment run will be addressed. The first thing was to have someone position the detectors at their corresponding angle settings using the angle readout settings in the vernier scale outside the chamber. This is shown in figure 1a. Then, the operator would set the energy settings for the alpha beam. The alpha beam is made from a Helium-4 isotope source called the duoplasmatron source [4]. As shown in figure 1b, the Helium-4 beam goes through a sequence of charge stripping/energy gain by the accelerator to become the specified alpha beam [4]. The alpha beam is directed toward the RBS station to begin the data collecting back-scattering and forward-scattering collection, which is shown in the DAQ system based on figure 1c. Other details to specify are that the charge integrator is what collects and specifies the total charge in the system, the scattering chamber encloses the station to prevent intermolecular reaction of air molecules and alphas, and the two detectors are what start the readout processes of taking an electrical signal to a digital pulse in a histogram/spectrum form [1]. [Counts: 185]

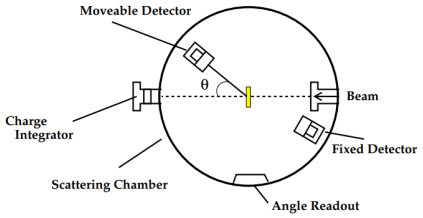

(a) Schematic of the Rutherford chamber for this experiment [1].

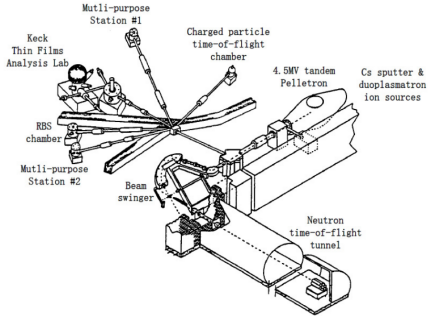

(b) Overview of the accelerator lab at Ohio University [4].

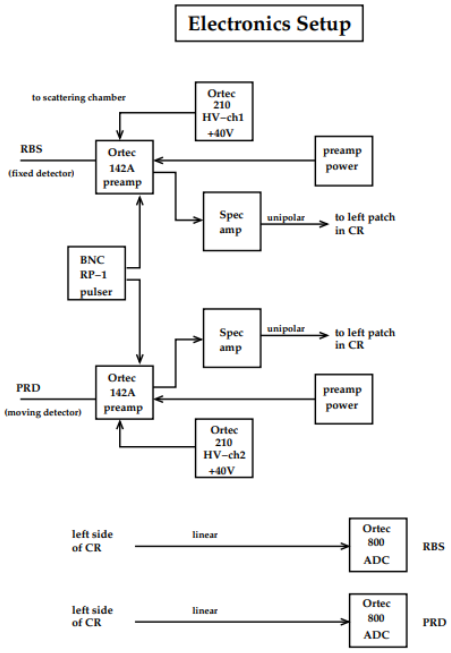

(c) Electrical setup showing how digitized counts are displayed [1].

Figure 1: Main components of this lab using the Edwards Facility at Ohio University to perform Rutherford Scattering experiments.

2.2 Pre-run Measurements

Figure 2 is a data collection table for solid angle calculations of the detectors. Figure 3 are the units used for this lab. Experimental differential cross-section units are defined by mb/sr. For the rest of this section, the convention of the detectors and data files is established. For both varying angle/energy data collection days, each data set is defined by a 4-tag.xy files, each ending with a number index. 000# are tag files for varying angle, and 100# for varying energy. the last digit that corresponds to 0,1, 2, and three in sequential order are the xy-files for the RBS, PRD, LT/DT, and BCI [5]. The only data files to use for offline analysis are the ones that correspond to RBS and PRD detectors. [Counts: 124]

Type	Name	Description
RBS	Distance	6.700 ± 0.035 cm
	Diameter	4.01 mm
	Angle (left)	$[225°, 335°]$
	Angle (right)	$[25°, 155°]$
PRD	Distance	6.075 ± 0.035 cm
	Diameter	3.69 mm
	Angle (fixed)	168°

Figure 2: Measurements taken from the RBS/PRD detectors and defining the angle ranges for the experiment [5].

$$1 \text{ barn} = 1 \text{ b} = 10^{-28} \text{ m}^2$$
$$1 \text{ millibarn} = 1 \text{ mb} = 10^{-31} \text{ m}^2$$

Figure 3: Units of area used in this lab [1].

2.3 Data Files to Process

Figures 4 and 5 are the data collected and organized from the DAQ system for varying angle and energy data ready to use for offline analysis. The final conventions to establish are that DTL is the dead times in percent form for the PRD detector and vice versa for the DTR association for the RBS detector. Other final notes for this section are that the fixed detector (RBS) was always established as $\theta = 168$ deg, and the movable (PRD) would vary or be set fixed based on a series of data runs. The detector angle is used as the scattering angle in this experiment, and essentially, if greater than $\theta > 90$ deg, the target is set to be $\theta = 0$ deg. If $\theta < 90$ deg, then the target is set to be half the detector angle. These are called back-scattering and forward-scattering processes. [Counts: 148]

Tag	$\theta_{\text{Det.}}$ [deg]	$\theta_{\text{targ.}}$ [deg]	I [nA]	BCI	DTL [%]	DTR [%]	Time [sec]
20	154.9	0	6	5000	1.0465	1.1628	86
30	60	30	6	5000	1.8391	1.3793	87
40	50	25	6	5000	5.4118	1.2941	85
50	40	20	6	5000	7.6136	1.25	88
60	-45 (215)	-22.5 (337.5)	6	5000	25.053	1.2629	95
70	-55 (305)	-27.5 (332.5)	6	5000	14.286	1.3187	91
80	-65 (295)	-32.5 (327.5)	6	5000	8.4043	1.276	94
90	-90 (270)	-45 (315)	6	5000	3.2673	1.2871	107
100	-90 (270)	-45 (315)	6	5000	3.8043	1.4130	92
110	-115 (245)	0	6	5000	1.5217	1.1957	92
120	-135 (225)	0	6	5000	1.1224	1.1224	98
130*	-35 (325)	-17.5 (342.5)	.6	5000	8.1818	0.56818	88
140*	30	15	.6	5000	10.28670	0.57143	105

(a) Data collection for varying angle data run [5].

Parameter	Value
E_{beam}	2.50 [MeV]
BCI Scale	10^{-8}
θ_{PRD}	168°

(b) Pre-definitions for angle varying data collection [5].

Figure 4: Collection of the tags, energies, scattering angles, BCI, and others for varying angle data collection [5].

Tag	E [MeV]	Θ_{RBS}	Θ_{Targ}	I [nA]	BCI	Scale [10^{-x}]	DTL [%]	DTR [%]	Time [sec]
1010	3.5	50.0 (1)	25.0 (5)	3	5000	8	1.9417	0.72816	206
1020	3.5	155.0 (1)	0.0 (1)	3	5000	8	0.46875	0.72917	192
1030	4.5	155.0 (1)	0.0 (1)	1.5	5000	8	0.34853	0.61662	373
1040	4.5	50.0 (1)	25.0 (1)	1.3	5000	8	0.96685	0.60773	373
1050*	6.5	50.0 (1)	25.0 (1)	1.5	10000	8	1.1679	0.024331	822
1060*	6.5	155.0 (1)	0.0 (1)	1.25	15000	8	0.027027	0.027027	1110

(a) Data collection for varying energy data run [5].

Type	Setting 1	Setting 2
θ_{PRD}	168°	168°
θ_{RBS}	50°	155°
θ_{Targ}	25°	0°

(b) Pre-definitions for energy varying data collection [5].

Figure 5: Collection of the tags, energies, scattering angles, BCI, and others for varying energy data collection [5].

3 Analysis/Results

The offline analysis performed was energy calibration of the system, composition confirmation, and theoretical vs. experiment Rutherford. This section will mainly focus on offline analysis of varying angle data. A quick note on uncertainty standards and error propagation will also be discussed at the end of this section. [Counts: 47]

3.1 Energy Calibration

In the first steps in the offline analysis, energy calibration was performed on the given peaks. Energy calibration for this report was done on PRD gold peaks corresponding to when $\theta_{\text{Detector}} = 155, 50$ and energies ranging from 2.5-6.5 MeV. Those peaks were chosen because of the following: peak separation, identification, and known physics, which the experimenter can guess by loading up the histograms to see. The overall steps in calibration used were: spectra/parameter processing of xy-files into a histogram, scattered energy calculation of the chosen peaks, using graphing/analysis software like ROOT to then plot the corresponding calibration plot with fit parameters extracted and performing residual calculation and plot to verify the quality of calibration fit-function. At the end of this subsection and the beginning of the next section, it will show how to extract the fit-calibration equation to extract copper and silver peaks for their centroid position. [Counts: 148]

Peak Processing

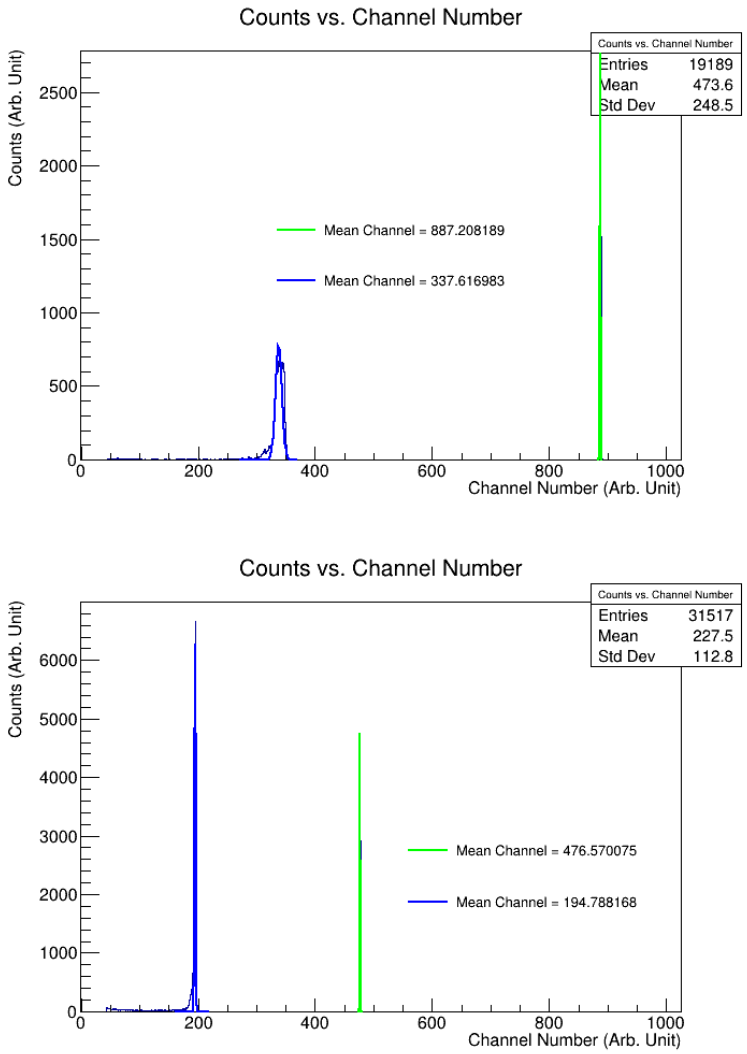

Figure 6: RBS and PRD-based tags that are Gaussian fitted and processed. The sharp peaks are the pulsars shown in the distribution, and the peaks with the exponential tails are the corresponding gold, silver, and copper peaks. Gold is more prominent in these tag files.

Figure 6 is part of the series of processed peaks, including composition-based Gaussian peaks fitted to obtain the mean position, counts, and corresponding uncertainties needed for plotting and calculations later. An important feature to mention with this stage is that the gold peaks were chosen for processing because the copper/silver peaks were not as displayed and tightly compacted within the left-sided exponential tail. The PRD tag files of the day-1 20s, 40s, and all day-2 100-based tags were used in the processing stage for calibration because of good variability that includes good data of forward and backward scattering processes. [Counts: 99]

Scattering Energy Calculation

$$E_{\text{att}} = \text{MSP} \times \frac{\text{Molar Mass}}{N_{\text{a}}} \times \text{CF} \times n_{\text{tar}} \tag{3}$$

$$E_{\text{f}} = E_{\text{i}} - E_{\text{att}} \tag{4}$$

$$E_{\text{avg}} = \frac{E_{\text{f}} + E_{\text{i}}}{2} \tag{5}$$

$$K = \left(\frac{M_0 \cos\theta + \sqrt{M_1^2 - M_0^2 \sin^2\theta}}{M_0 + M_1} \right)^2 \tag{6}$$

$$E_{\text{sc}} = E_{\text{avg}} \times K \tag{7}$$

After peak processing, Equations 3 - 7 are how the beam's energy after scattering was obtained, and those values are used in the calibration plotting. The underlying physics to think about here in this step is that when the alphas for each trial impinge the foil target, they first give off energy based on other interactions with the nuclei within the foil and then, based on the potential of the target is what gives the final scattering energy. To get the uncertainties of the scattered energy error-propagation of equations 6, and 7 were performed starting with uncertainty contribution of θ within 1-degree. [Counts: 108]

Calibration Results/Residual Testing

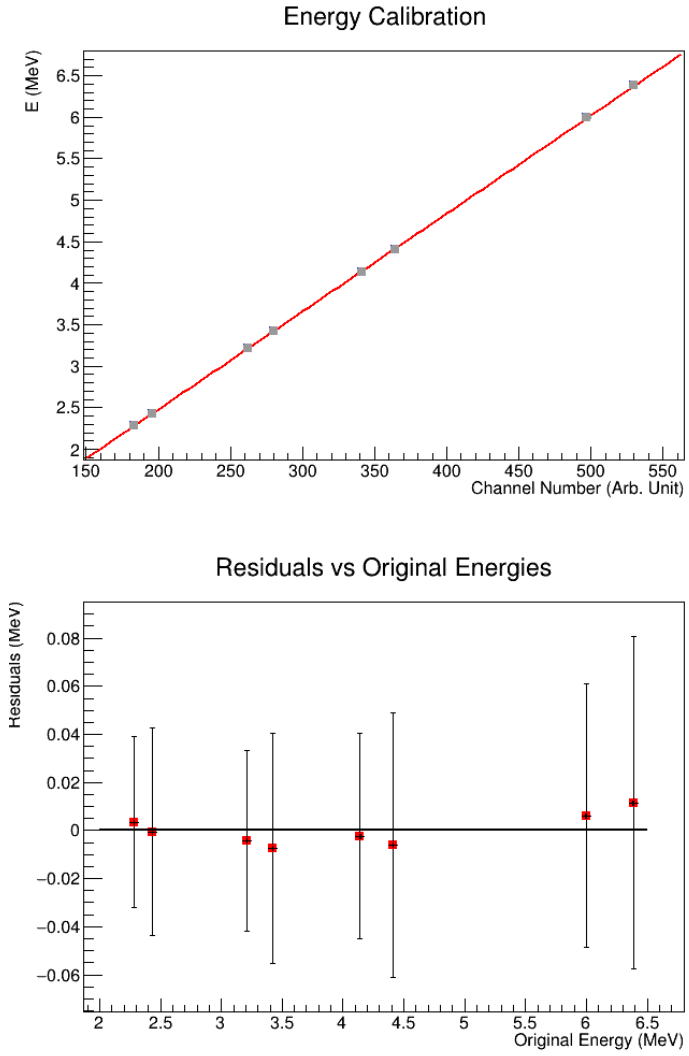

Figure 7: The resultant energy calibration plot for the detectors and residuals plot for verification.

$$E_{\text{cal}} = \text{a} \times \text{x} + \text{b} \tag{8}$$

- a = 0.0118092 ± 0.0000048
- b = 0.1172 ± 0.0013

Once the mean bins, scattered energies, and uncertainties were obtained, figure 7 and equation 8 are the resultant plots and fit parameters obtained. What is noticeable at the end of this step is the residuals for gold peaks of the detector system range from -0.1 to 0.1 Mev, which show acceptable standards of trusting equation 8. This is helpful in the next stage because this calibration fit can

reasonably help obtain peak positions of silver and copper for composition confirmation. Table 1 is the data collected for the calibration process. [Counts: 91]

Table of all Calibration Data/Step

Tags Used	θ_{Det}	E_{i} (MeV)	Mean Bin	N_{s} (Counts)	E_{sc} (MeV)	E_{Cal} (MeV)	R (MeV)
tag0021	155.0(1)	2.5	183.10(4)	9984(16)	2.283(1)	2.279(1)	0.004(36)
tag0041	50.0(1)	2.5	196.00(1)	55917(110)	2.431(1)	2.432(1)	-0.001(43)
tag1011	50(1)	3.5	280.42(1)	54386(235)	3.421(2)	3.429(1)	-0.008(48)
tag1021	155(1)	3.5	262.46(4)	4836(72)	3.212(1)	3.217(1)	-0.005(37)
tag1031	155(1)	4.5	340.91(5)	2897(55)	4.141(1)	4.143(1)	-0.002(43)
tag1041	50(1)	4.5	364.02(2)	2381(59)	4.410(2)	4.416(1)	-0.006(55)
tag1051	50(1)	6.5	529.78(2)	3136(66)	6.385(3)	6.373(1)	0.012(69)
tag1061	155(1)	6.5	497.24(4)	4365(67)	5.995(2)	5.989(1)	0.006(55)

Table 1: This is all the data obtained from ROOT's fitting processes, developed algorithms, and plotting steps applied for the calibration analysis.

3.2 Composition Confirmation

In composition confirmation, the goal for this processing step was if, assuming your experiment system follows the theoretical Rutherford Model, the composition confirmation can be reaffirmed. With this understanding, the goal was to get compositions within acceptable ranges for 80 %, 10 %, and 10% requirements of gold, silver, and copper. Since the system assumes ideal Rutherford conditions, then manipulations of equations 1 and 2 can be manipulated to get a composition relation that can be used for gold, silver, and copper. The calibration equation equations and scattering energy processes are first used to find the peak positions of silver and copper within the given PRD dataset. In this analysis, the PRD 6.5 MeV back-scattering process data was used because of good peak separations of silver and copper. Once all that is done, applying said information to composition equations gives the compositions. [Counts: 145]

Composition Algorithm

$$f_{Y/X} = \frac{N_Y \left(\frac{d\sigma}{d\Omega}\right)_X}{N_X \left(\frac{d\sigma}{d\Omega}\right)_Y} \tag{9}$$

$$f_X = \frac{1}{1 + f_{Y/X} + f_{Z/X}} \tag{10}$$

Once the mean positions are found in the corresponding peaks, then the compositions of gold, silver, and copper can be re-derived by applying equations 9 and 10 to each peak. Equation 9 is explicitly found by applying the count's parameters by fitting with the tag file of interest and by applying 2. The set's composition can be obtained once all the partial ratios are found in the specific gold, silver, and copper series. [Counts: 73]

Composition Results

Gold Comp %	Silver Comp %	Copper Comp %
79.3(1.1)	10.99(63)	9.72(94)

Table 2: Composition found for gold, copper, and silver contributions.

The interesting results of table 2 are that the compositions found are approximately close to the requirement and are at least within 0.1σ to 1σ. With this result, it confirms the confirmation. [Counts: 32]

3.3 Theory Vs. Experiment

This lab step aimed to plot one of the theoretical/experimental Rutherford's cross sections vs. an absolute scale of scattering angles (Detector angles). This plot uses only the gold peaks considered and shows how close the experimental and theoretical cross-section data are. This means to prove $\sin^{-4}_{\theta/2}$ dependency of the experimental cross-sections. Another test was to take experimental and theoretical values as divided ratios and plot that on this same angle scale to see a more concrete test of the fraction composed of the data. For example, if the ratios on average converged to 1.0, then that would mean perfect agreement. The absolute scale of angles meant that all plots were plotted from the range of $0 \leq \theta_{\text{sc}} \leq 180$ degrees. All calculations used the given scattering angles for processing cross sections but were converted to meet this absolute scale by applying a subtraction of 360 degrees, then taken absolute if needed. To calculate the theoretical cross-section, they are defined by equation 2. To calculate experimental cross-section, they are defined by equation 1. More specifically, the experimental cross-section is determined using the following: the signal count is corrected for dead times, the incident count is derived from BCI charge conversion, the solid angle is calculated based on PRD, and the target density is adjusted for angular corrections, composition percentages, and unit conversions. [Counts: 220]

The critical result for figure 8 is that the dead times when the detector angle was 30, 40, and 60 degrees were off in collecting scattering events. This effect, especially for the first plot, still doesn't change the precise result, stating that the experimental curve has $\sin^{-4}_{\theta/2}$ dependency. A correction for the lousy angle dead times was performed. It improved the $\sin^{-4}_{\theta/2}$ dependency, showing that the gold peaks for day-1 data improve Rutherford assumptions, showing that the experiment gold peaks qualify Rutherford Model assumptions and improving the $\sin^{-4}_{\theta/2}$. In the last plot, most of the

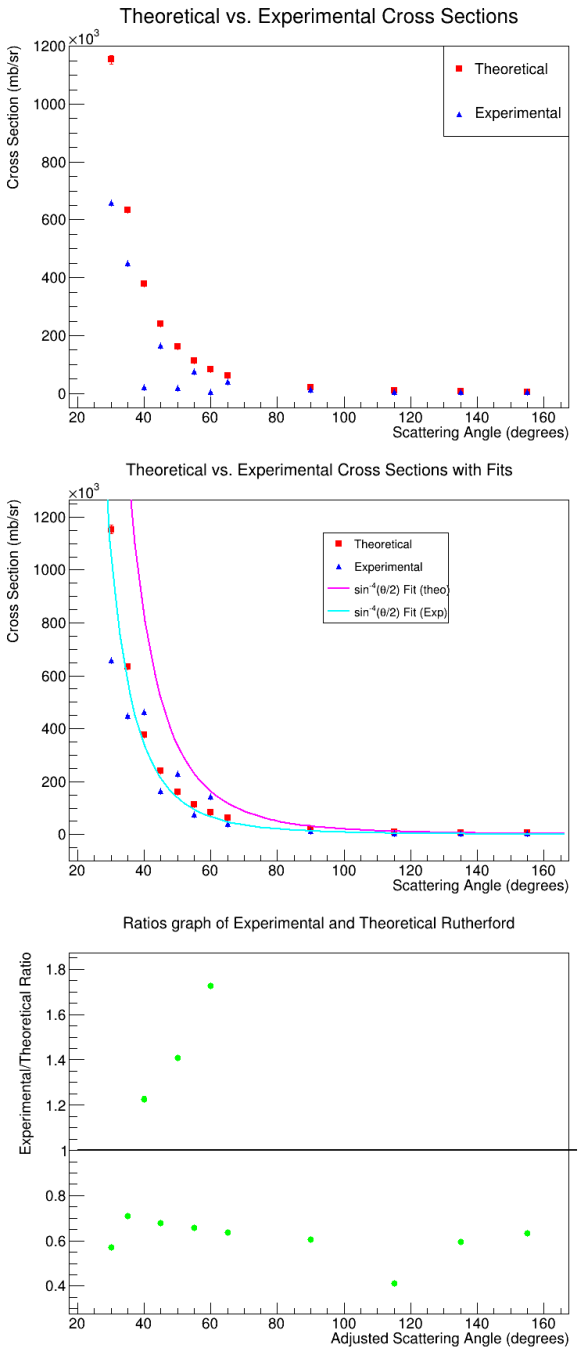

Figure 8: Plot of Rutherford cross-sections versus angle displaying before and after dead-time corrections for θ_{DET} = 30, 40, and 60 degrees. The ratio of experimental and theoretical per scattering angle plot.

ratio of cross-section converged to 0.7, which means only a 30 % discrepancy between theory and experimental values. [Counts: 115]

3.4 Uncertainties/Error Propagation Processes

$$(\Delta Q)^2 = \sum_{i=1}^{n} \left(\frac{\partial Q}{\partial x_i} \Delta x_i \right)^2, \tag{11}$$

Where:

- Q is a function of independent variables $x_1, x_2, \ldots, x_n$: $Q = f(x_1, x_2, \ldots, x_n)$,
- $\frac{\partial Q}{\partial x_i}$ is the partial derivative of Q with respect to x_i,
- Δx_i is the uncertainty in x_i,
- The uncertainties Δx_i are assumed to be independent and uncorrelated.

For this lab, uncertainties were categorized as measure uncertainties, uncertainties obtained from databases, and uncertainties derived by 11. For measured uncertainties specifically from the lab, angles were measured, and it was important to note that for day 1, angle uncertainties were defined as 0.1 degrees and 1 degree for day 2 [5]. For masses, mass-stopping power uncertainties were obtained from databases [6], [7]. Lastly, uncertainties were obtained for calculated processes by applying equation 11 to all other equations. [Counts: 78]

4 Conclusion

This lab was done to introduce the ideas of Rutherford's Scattering to the accelerator lab here at Ohio University and to see how it could compare to theoretical predictions. To reiterate, the tasks that were completed were calibration, Composition confirmation of the target, and theoretical/experimental cross-section comparisons. Calibration was done successfully because of residuals ranging from $-0.1 \leq R \leq 0.1$ Mev, the residuals plot converging to a constant line, and the finding of less prominent copper/silver peaks from tag 1061. For compositions, they approximately matched the 80 %, 10 %, and 10% requirements for gold, silver, and copper. The comparisons for both experimental and theoretical plots had the same distribution except for angle ranges from $30 \leq \theta_{\text{sc}} \leq 60$ degrees because of incorrect dead-times values. The ratio plots of cross sections converged approximately to $R = 0.7$, which shows a close approximation of theoretical and experimental cross sections with only a 30 % discrepancy. The only thing that could be improved from this report is to have longer run times and to see how the dead times for those angle ranges were incorrect. [Counts: 183]

Works Cited

[1] Dr. Paul King. *Physics 6751: Nuclear Lab Manual*. Version 24.5. Athens, Ohio, 2024.

[2] John R. Taylor. *Classical Mechanics*. Collisions, Central Force Problem. Sausalito, CA: University Science Books, 2005. Chap. 14, 8.

[3] Nouredine Zettili. *Quantum Mechanics: Concepts and Applications*. 2nd. Scattering Theory. Wiley, 2009. Chap. 11.

[4] Zach Meisel et al. "The Edwards Accelerator Laboratory at Ohio University". In: *Physics Procedia* 90 (2017). Presented at the Conference on the Application of Accelerators in Research and Industry (CAARI 2016), Ft. Worth, TX, USA., pp. 448–454. DOI: 10.1016/j.phpro.2017.09.050.

[5] Ryan Conaway and Unish Gautam. *Rutherford: Lab Notes*. Lab Notes. Published on November 7, 2024. 2024. URL: N/A.

[6] International Union of Pure and Applied Chemistry (IUPAC). *Standard Atomic Weights 2021*. Accessed: 2024-11-27. 2024. URL: https://iupac.qmul.ac.uk/AtWt/.

[7] National Institute of Standards and Technology (NIST). *Stopping-Power and Range Tables for Electrons, Protons, and Helium Ions (ASTAR)*. Accessed: 2024-11-27. 2024. URL: https://physics.nist.gov/PhysRefData/Star/Text/ASTAR.html.